Title

Kindlin Is Mechanosensitive: Force-Induced Conformational Switch Mediates Cross-Talk among Integrins

Journal

Biophysical Journal, 116(6)

ISSN

0006-3495

Authors

Jahed, Zeinab
Haydari, Zainab
Rathish, Akshay
et al.

Publication Date

2019-03-01

DOI

10.1016/j.bpj.2019.01.038

Peer reviewed

Biophysical Journal
Article

Biophysical Society

Kindlin Is Mechanosensitive: Force-Induced Conformational Switch Mediates Cross-Talk among Integrins

Zeinab Jahed,[1] Zainab Haydari,[1] Akshay Rathish,[1] and Mohammad R. K. Mofrad[1,2,*]
[1]Molecular Cell Biomechanics Laboratory, Departments of Bioengineering and Mechanical Engineering, University of California, Berkeley, California and [2]Molecular Biophysics and Integrative Bioimaging Division, Lawrence Berkeley National Laboratory, Berkeley, California

ABSTRACT Mechanical stresses directly regulate the function of several proteins of the integrin-mediated focal adhesion complex as they experience intra- and extracellular forces. Kindlin is a largely overlooked member of the focal adhesion complex whose roles in cellular mechanotransduction are only recently being identified. Recent crystallographic experiments have revealed that kindlins can form dimers that bind simultaneously to two integrins, providing a mechanistic explanation of how kindlins may promote integrin activation and clustering. In this study, using the newly identified molecular structure, we modeled the response of the kindlin2 dimer in complex with integrin β1 to mechanical cytoskeletal forces on integrins. Using molecular dynamics simulations, we show that forces on integrins are directly transmitted to the kindlin2 dimerization site, resulting in a shift in an R577-S550/E553 interaction network at this site. Under force, R577 on one protomer switches from interacting with S550 to forming new hydrogen bonds with E553 on the neighboring protomer, resulting in the strengthening of the kindlin2 dimer in complex with integrin β1. This force-induced strengthening is similar to the catch-bond mechanisms that have previously been observed in other adhesion molecules. Based on our results, we propose that the kindlin2 dimer is mechanosensitive and can strengthen integrin-mediated focal adhesions under force by shifting the interactions at its dimerization sites.

INTRODUCTION

Among adhesion proteins, integrins are of crucial importance because they serve as the primary receptors for mechanical signals sensed by the cell. Integrins are a family of heterodimeric transmembrane proteins that are composed of α- and β-subunits that bind to extracellular matrix proteins (1,2). Each integrin subunit consists of a large extracellular domain, a single-pass transmembrane helix, and a short cytoplasmic tail (Fig. 1 *A*). Integrins play critical roles in a variety of cell functions, including linking focal adhesion assemblies to the extracellular microenvironment, facilitating cell migration, transmitting signals bidirectionally, and controlling cell growth, stem cell differentiation, and apoptosis (3–5). Integrin may be activated by mechanical or biochemical signals within the cell ("inside-out signaling") or by mechanical stresses generated in the extracellular domain ("outside-in signaling") (6–8).

Integrin activation

There are two distinct and conserved NxxY (x represents any amino acid) binding sites on the β-integrin cytoplasmic tails. It is now widely accepted that talin and kindlin cooperate to change integrin conformation from the bent (inactive, low-affinity state) to an extended (active, high-affinity state) conformation upon binding to the membrane proximal and membrane distal NxxY motifs, respectively (Fig. 1 *A*). Moreover, talin and kindlin are required for maintaining the extended conformation of integrins (9–12). There has been a long-standing hypothesis that kindlin may also be involved in the clustering of activated integrins (13,14). The crystal structure of kindlin2 in complex with integrin was recently solved in 2017 and provided valuable insights into molecular mechanisms of kindlin's involvement in integrin activation and clustering (14). It was suggested that kindlin2 could form dimers that can bind to two integrins simultaneously (Fig. 1 *A*). This observation

Submitted August 10, 2018, and accepted for publication January 22, 2019.
*Correspondence: mofrad@berkeley.edu
Zeinab Jahed and Zainab Haydari contributed equally to this work.
Editor: D. Peter Tieleman.
https://doi.org/10.1016/j.bpj.2019.01.038

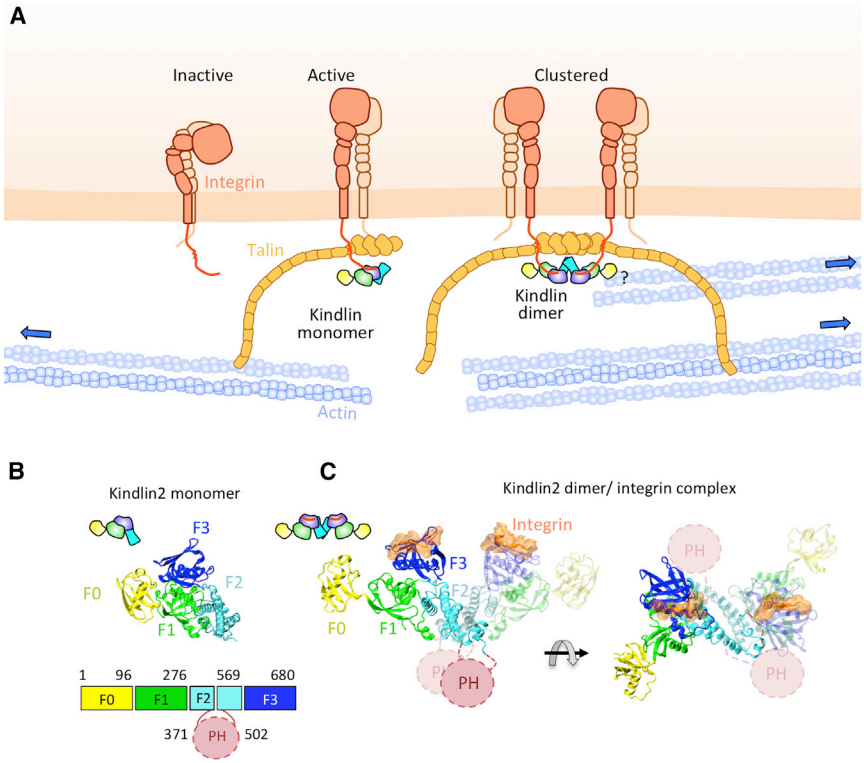

FIGURE 1 Kindlin in the integrin-mediated adhesion complex. (*A*) A schematic representation of integrin activation and clustering is shown. Talin and kindlin are both involved in the activation of integrin. Talin binds to the actin cytoskeleton and provides a linkage between the extracellular environment and the cytoskeleton. Kindlin dimerization is also important for integrin activation and clustering. (*B*) The structure of kindlin2 monomer (PDB: 5XPY) and its cartoon representation matching (*A*) is shown. The sequence location of each domain is shown on the bottom. (*C*) The structure of kindlin2 dimer in complex with integrin-β1 (PDB: 5XQ0) and its cartoon representation matching (*A*) is shown. The important structural domains are identified with various colors. To see this figure in color, go online.

provided a mechanistic explanation for how kindlins may promote integrin clustering.

Role of mechanical forces

A central requirement for focal adhesion assembly, growth, and function are forces generated within the cell. The integrin adhesion complex is linked to the actin cytoskeleton through several adaptor proteins and hence experiences mechanical forces generated by the actin retrograde flow and myosin II (8,15–17). A vast body of evidence indicates that mechanical stresses directly regulate the function of several focal adhesion proteins, including integrin, filamin, talin, vinculin, and focal adhesion kinase (7,18–25). As a result, several studies have focused on characterizing the response of these proteins to force (18–21,23,24,26–28). Despite the central role of kindlin in the integrin-mediated adhesion complex, kindlin has been largely overlooked when exploring the mechanosensitive properties of focal adhesions. Hence, little is known about the molecular mechanisms of kindlin's involvement in focal adhesion formation and function and its response to mechanical forces at adhesion sites. Recent works show that kindlin is in fact involved in cellular mechanotransduction (29,30). There is also direct evidence that forces from actin are responsible for integrin activation and that tension on integrins is dependent on interactions with both talin and kindlin (11). Forces on integrins emerge internally through their connection with the actin cytoskeleton or externally through phenomena such as shear flow in blood vessels or matrix stretching (28,31,32). There is also some evidence that kindlin contains an actin binding site that can directly bind to the actin cytoskeleton (33). The recent discovery that kindlin2 can form dimers that simultaneously bind two integrins raises the question of how the kindlin2 dimer complex responds to mechanical forces on integrins. In this study, we present the first, to the best of our knowledge, model explaining the mechanisms of kindlin's response to force.

Crystal structure of dimeric kindlin2 in complex with integrin-β1

Kindlin belongs to a family of evolutionarily conserved proteins, including kindlin-1, -2, and -3. Like talin, kindlin is a FERM (protein4.1, ezrin, radixin, and moesin) domain containing protein. FERM domain is composed of three subdomains: F1, F2, and F3. Compared to typical FERM domain proteins, kindlin FERM contains an additional F0 domain (N-terminus) and a pleckstrin homology domain inserted into the F2 subdomain (Fig. 1 *B*). Although different kindlins exhibit high sequence similarities, they often present tissue-specific distributions (8,9,34). Recent crystallography data on kindlin2 demonstrated that it can form homodimers through its F2 domain in a domain-swapped manner (Fig. 1 *C*), and that the structures of the kindlin2 monomer and dimer vary in a single α-helix in the F2 domain, whereas all other domains are identical (14).

Using the recently solved crystal structure of the dimeric kindlin2 (referred to as kindlin2dimer) in complex with integrin-β1, we develop all-atom molecular dynamics (MD) models to examine the response of the kindlin2dimer to mechanical forces on integrins. Our results show that forces on integrins are directly transmitted to the kindlin2dimer interface and induce a shift in the interactions at this interface, which strengthens the kindlin2dimer under force. Based on our results, we propose kindlin as a new, to our knowledge, member of the load-bearing and mechanosensitive proteins of integrin-mediated focal adhesions.

MATERIALS AND METHODS

NMA

To predict the large-scale functional motions of the kindlin2dimer/integrin-β1 modeled structure, we first performed a normal mode analysis (NMA) and calculated the most prevalent atomic fluctuations averaged among all modes (Fig. S1). For this study, the Bio3D package in R was utilized to conduct the NMA analysis and produce visualizations of the data (35). A variety of functions from the Bio3D package were employed, including *nma.pdbs()* function to calculate the normal modes and produce an NMA object. Subsequently, a cross correlation analysis was conducted using the *dccm.nma()* function that required the NMA object as an input to produce the correlation map. The Bio3D package also allowed for visualization between correlated residues in PyMol (36) using the *pymol()* function. This function created a three-dimensional visualization of the kindlin2dimer/integrin-β1 model and highlighted key correlated and anticorrelated residues between the different subdomains (as shown in Fig. 2). A total of 2532 modes were obtained, including the first 6 modes (trivial modes) with 0 frequencies, which correspond to rigid-body rotation and translation. The average fluctuation of the molecule was calculated using the *fluct.nma()* function (35), which calculates the average fluctuations over all modes weighted by the corresponding eigenvalues (Fig. S1).

Structural model of the kindlin2dimer

The crystal structure of the kindlin2dimer bound to two integrins was obtained from the Protein Data Bank (PDB: 5XQ0). This crystal structure includes residues 787–797 of integrin-β1, which are bound to the F3 subdomain of the kindlin2dimer (14). The solved crystal structure of the kindlin2dimer is missing two regions. Specifically, the residues missing from the structure are residues 168–217 in the F1 subdomain and residues 337–512 in the F2 subdomain. Because these missing regions are linked to the solved structure via flexible linkers, the motions of these missing regions are supposedly independent from the other parts of the molecule (14). Therefore, we also excluded these unsolved regions from our models to reduce the introduction of uncertainties resulting from homology modeling. Next, to resemble the cellular environment more closely, the kindlin2dimer/integrin-β1 structure was solvated in explicit water. The TIP3P model was used for water molecules (37). The solvation was performed using NAMD solvate package, using a 2.4-Å boundary. The size of the solvation box was determined by subtracting or adding 20 Å to the minimal and maximal values of x, y, and z coordinates of the protein, respectively. To simulate the cytoplasmic environment, the system was neutralized with counterions and ionized with 150 mM of KCl. The final system with the protein, water, and ions consisted of 276,045 atoms.

MD simulations and analyses

We used all-atom MD simulations to model the response of the kindlin2dimer to force. All-atom MD simulations for this study were performed using NAMD scalable MD with the CHARMM force field and visualized using visual MD (VMD) (38,39). To remove any nonphysical contacts or interactions, the system was minimized at 100,000 steps. Before applying forces, we equilibrated the system for 25 ns with a time step of 2 fs. The hydrogen atom bond length was constrained using the SHAKE method (40). The SHAKE algorithm is used to constrain bond lengths between heavy atoms and hydrogen atoms. Simulations were performed under a constant temperature of 310 K and a constant pressure of 1 atm using the Langevin piston method (50 fs decay time) and Hoover's method during minimization and equilibration (39). Periodic boundary conditions were applied in all three directions, and particle mesh Ewald was used with a 1 Å maximal space between grid points (39). The cutoff for nonbonded interactions was set to 12 Å. A switching function was used for all calculations with a switching distance of 10 Å.

For the constant-velocity pulling simulations, a dummy atom was attached to the position of the center residue (V787) at the N-terminal end of the integrin-β1 tail bound to protomer 1 (I1) via a virtual spring with a spring constant of 7 kcal/mol/Å^2; the position of residue V787 on protomer 2 (I2) was fixed. The constant velocity simulations were performed at a constant pulling rate of 0.5 Å/ns. We then measured the forces between the dummy atom and

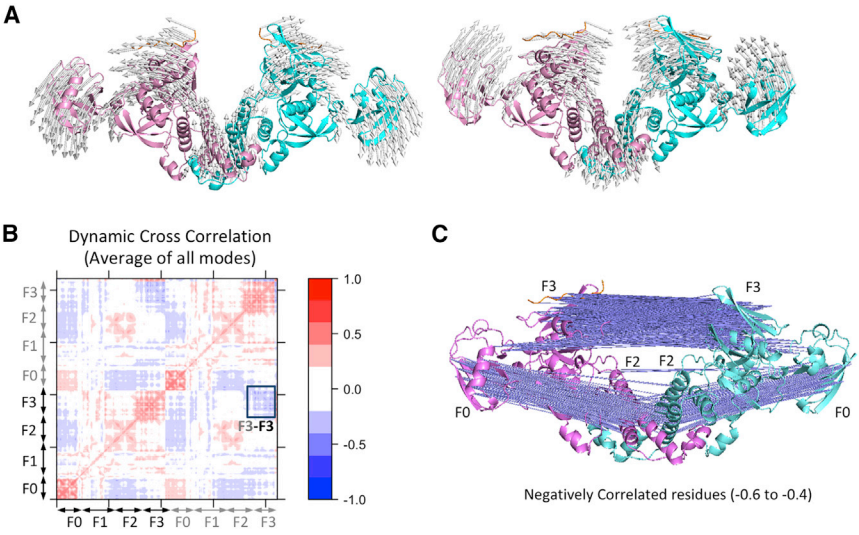

FIGURE 2 Normal mode analysis (NMA) of the kindlin2dimer. (*A*) Vector field representation of first nontrivial normal mode from NMA is shown. (*B*) A dynamic cross correlation heat map of the kindlin2dimer averaged over all modes is shown. F0, F1, F2, and F3 subdomain regions are indicated on the heat map; black labels represent the F0–F3 subdomains of protomer 1 (*magenta*), and the gray labels represent the F0–F3 subdomains of protomer 2 (*cyan*). A black box is drawn to indicate that the F3 subdomains of two protomers in the kindlin2dimer that bind to integrin are negatively correlated. (*C*) A visualization of negatively cross correlated residues on the kindlin2dimer is shown. Each negatively correlated residue is connected with a blue line. Residues on F3 subdomains of the kindlin2dimer are negatively correlated with each other. To see this figure in color, go online.

V787 using NAMD (39). The kindlin2dimer was subjected to both tensile and compressive strains, and residue distances and angles were calculated and visualized using VMD and R (35). To calculate average forces, we first reduced the noise from the measurements obtained from our MD simulations. To do this, we used the filter function in R to calculate a moving average of forces. The filter function was also used to reduce the noise in the distance and angle plots (a window of 10 frames was used for averaging). Tensile and compressive strains were applied to the kindlin2dimer/integrin-β1 complex for 50 ns, and the protein was relaxed for another 100 ns. Each condition was repeated three times (see summary of simulations in Table 1).

In the constant-force simulations, a specific, constant force (namely 87, 70, 35, and 17 pN) was applied on residue V787 of one integrin in the kindlin2dimer/integrin-β1 complex (I1), while the V787 of the other integrin (I2) was fixed. Tensile forces were applied in these simulations (see summary of simulations in Table 1). The distances were calculated as stated above.

Comparison between MD simulations and NMA

Squared overlap analysis was carried out to determine which normal modes contribute to the conformational changes observed in our MD simulations. We calculated the squared overlap of the first 20 normal modes, with the conformational difference vector between the first and last frames of our MD trajectories where tensile or compressive forces were applied (0 and 50 ns). These calculations were performed using the Bio3D package in R (35,41). To compare the normal modes of the protein to the protein conformations during MD simulations where forces were applied (0–50 ns), we calculated the root mean-square inner product (RMSIP) of the normal modes obtained from NMA and the principal components obtained from MD simulations, using the Bio3D package in R (35,41).

H-bond calculations

The number of hydrogen bonds (H-bonds) between regions of interest were also calculated in VMD using the H-bonds plug-in (version 1.2) (21,39) in which the cutoff distance and angle were set to 3 Å and 20°, respectively. The density- and time-dependent plots were all prepared in R matrixStats and gplots (42,43).

In all reported data, a Welch's two-sample *t*-test was conducted using R Stats Package (version 3.5.0) to test for statistical significance.

RMSD and RMSF analyses

The root mean-square deviation (RMSD) values of the kindlin2dimer were quantified for each simulation using the RMSD visualizer tool in VMD (21). The movements of the molecule due to rotation and translations were suppressed by aligning the kindlin2dimer of all frames of the trajectory to a reference frame (frame 0).

The root mean-square fluctuation (RMSF) values were calculated using the *rmsf()* function in R Bio3D package (35). Before RMSF calculations, the movements of the molecule due to rotation and translations were suppressed by using the *fit.xyz()*. In MD simulations, RMSF is a good measure of conformational variance, which compares the fluctuations of each residue from a mean position of the residue averaged over MD simulation time. Free-hanging end regions of the molecule that are not connected to other regions usually exhibit very high RMSF values and were therefore ignored in our analyses.

Force distribution analysis

Time-resolved force distribution analysis was performed using the TRFDA GROMACS tool (44). Using this tool, atomic pairwise forces were calculated for Coulomb interactions and monitored over simulation time. The methods for pairwise force calculations are described in detail in (45). Briefly, the interaction between residues r_i and r_j (where i and j are atoms of each residue) is represented by a pairwise force acting on the center of mass of the two residues, which is calculated using the following equation:

$$\vec{F}_{ri,\,rj} = \sum_{ieri,\,ierj} \vec{F}_{ij}.$$

Punctual stresses for each residue were then calculated using the GROMACS's *fda_get_stress* function. This function calculated the punctual stress by summing the absolute values of the pairwise forces acting on each atom (44).

Cumulative distance change calculation

To determine how the R557-E553/S550 conformational switch affects the distance change between integrins under force, we calculated the cumulative distance changes between two integrins before and after the conformational switch event for all of our simulations in which a constant force was applied. Specifically, we calculate iterated differences between the distances of V787 of I1 and I2 using the *diff()* function in R with a lag value of 1. We then summed up these values to obtain cumulative distances. For each force magnitude, the cumulative distance was evaluated before and after the α-carbon (Cα) atoms of R557 and E553 reach a value of 13.75 Å.

RESULTS

Dynamic cross correlation of domains of kindlin protomers in the kindlin2dimer

To explore the structural dynamics of the kindlin2dimer, we first calculated the normal modes of the kindlin2dimer/

TABLE 1 Summary of Models Presented in This Manuscript

Modeled System	Number of Runs	Total Time of Force Application (ns)	Total Time of Relaxation (ns)
Tension: constant velocity (0.5 Å/ns)	run 1	50	~90
	run 2	50	~90
	run 3	50	~90
Compression: constant velocity (0.5 Å/ns)	run 1	50	100
	run 2	50	100
	run 3	50	100
Tension: constant force (87 pN)	run 1	55	–
	run 2	82	–
Tension: constant force (70 pN)	run 1	68	–
Tension: constant force (35 pN)	run 1	48	–
Tension: constant force (17 pN)	run 1	234	–
No force	run 1	–	~120

integrin-β1 complex (Fig. S1; Video S1). The lowest frequency nonrigid body motions of the kindlin2dimer consists of lateral contraction and expansion of the kindlin2dimer (Fig. 2 *A*). These motions resulted in an increase or decrease in the lateral distance between the two bound integrins (Video S1). Additionally, we performed dynamic cross correlation analysis between all residue pairs on the kindlin2dimer as obtained from the average of all modes in the NMA. Of particular interest was a coupling (i.e., anti-correlated motions) between the F3 domains of the two kindlin2 protomers in the kindlin2dimer (Fig. 2, *B* and *C*). Note that the two integrins are also bound to the F3 domains (Fig. 1), implying their motions are negatively correlated through the kindlin2dimer.

Kindlin2dimer responds to forces on integrin

The β1 tail of integrin is bound to talin at its membrane proximal region, and to kindlin at its membrane distal region (Fig. 1 *A*). To model the effect of mechanical forces on the integrin adhesion complex on the conformation of the kindlin2dimer, we used MD simulations to apply steering forces at a constant velocity of 0.5 Å/ns on residue V787 at the N-terminal end of the integrin tail bound to P1 (denoted as I1 in Fig. 3 *A*) and fixed the position of the same residue of the integrin tail bound to P2 (denoted in Fig. 3 *A*). These forces were applied in two tensile and compressive directions, which would result in an increase or decrease in the distance between I1 and I2, respectively.

After the application of forces for 50 ns (equivalent to a 25-Å change in the distance between I1 and I2), forces were removed, and the molecule was relaxed for 100 ns (Fig. 3, *B* and *C*). A control simulation was also performed with no force on the kindlin2dimer. As expected, the MD trajectories show a 25-Å change in the distance between I1 and I2 during force application in all simulation runs (Fig. 3, *B* and *C*). The initial distance between I1 and I2 was measured as ~75 Å, and upon force application, this distance increased to 100 Å under tensile forces or decreased to 50 Å under compressive forces (Fig. 3 *C*). Interestingly, even in our control simulation, where no forces were applied, the distance between I1 and I2 fluctuated between 58 and 78 Å during the simulation time. Upon the removal of tensile forces, the distance between I1 and I2 abruptly drops and stabilizes at a value of 73.5 ± 4.2 Å in the last 75 ns. On the other hand, after the removal of compressive forces, the distance between I1 and I2 increases slightly but continues to fluctuate significantly and reaches an average value of 65.5 ± 5.5 Å in the last 75 ns. These values are statistically indistinguishable from the distance between I1 and I2 in the no-force control simulation (66.6 ± 3.5 Å). Our results show that after tensile forces are applied and removed, the distance between I1 and I2 increases by a value of ~6 Å as compared with the no-force control simulation. In the case of compressive forces, there is no significant change in the distance between I1 and I2 compared with no-force conditions (Fig. 3 *C*).

Next, to investigate how the application of tensile and compressive forces alters the overall structure of the kindlin2dimer, we calculated the RMSD of the kindlin2dimer over the simulations time with respect to its initial structure before application of force (Fig. 3 *C*). The kindlin2dimer exhibited a tensile-force-dependent increase in RMSD, which reduced to its original value upon force removal. On the other hand, the kindlin2dimer RMSD appeared independent of force in compressive force simulations. Based on the RMSD values, our results suggest that forces resulting in the separation of integrins by ~25 Å (tensile forces) can induce significant structural changes in the kindlin2dimer, but these changes are mostly reversible after forces are removed (Fig. 3 *C*). Alternatively, the distance between two integrins can be decreased by ~25 Å (compressive forces) without a significant change in kindlin2dimer structure after force removal (Fig. 3 *C*).

To compare the amount of the force required to increase or decrease the distance between two kindlin-bound integrins in our MD simulations, we calculated the range of forces required to change the distance between I1 and I2 at a constant velocity (Fig. 3 *D*). Our results show that decreasing the distance between I1 and I2 by ~25 Å requires a lower range of forces (36 ± 41 pN) than pulling them apart by ~25 Å (90 ± 68 pN) (Fig. 3 *D*).

Next, we asked whether any of the normal modes could contribute to the conformational changes observed in tension and compression MD simulations (i.e., increase or decrease the distance between two kindlin-bound integrins). We calculated the squared overlap between the nontrivial normal modes of the kindlin2dimer and the conformational difference vector between the initial and final frames of the MD simulations of the kindlin2dimer under force (i.e., frames 0 and 50 ns) (Fig. 3 *E*). The first nontrivial mode (Video S1) exhibited high-squared overlap with the conformational difference vector in both tension and compression (Fig. 3 *E*). The third nontrivial mode (Video S2) contributed exclusively to tension and not compression simulations (Fig. 3 *E*). No other mode from the first 20 nontrivial normal modes showed any overlap with MD simulations. Finally, to compare the MD results with our NMA results, we compared the normal modes of the kindlin2dimer with the projection of MD conformers onto principal components (Fig. 3 *F*). The RMSIP of the 10 first modes of NMA and the 10 first principal components of MD principal component analysis (PCA) yielded a value of 0.82 and 0.83 for tension and compression, respectively (Fig. 3 *F*). These results suggest a very similar directionality between NMA modes and conformations obtained from MD simulations (a value of 1 would indicate identical directionality).

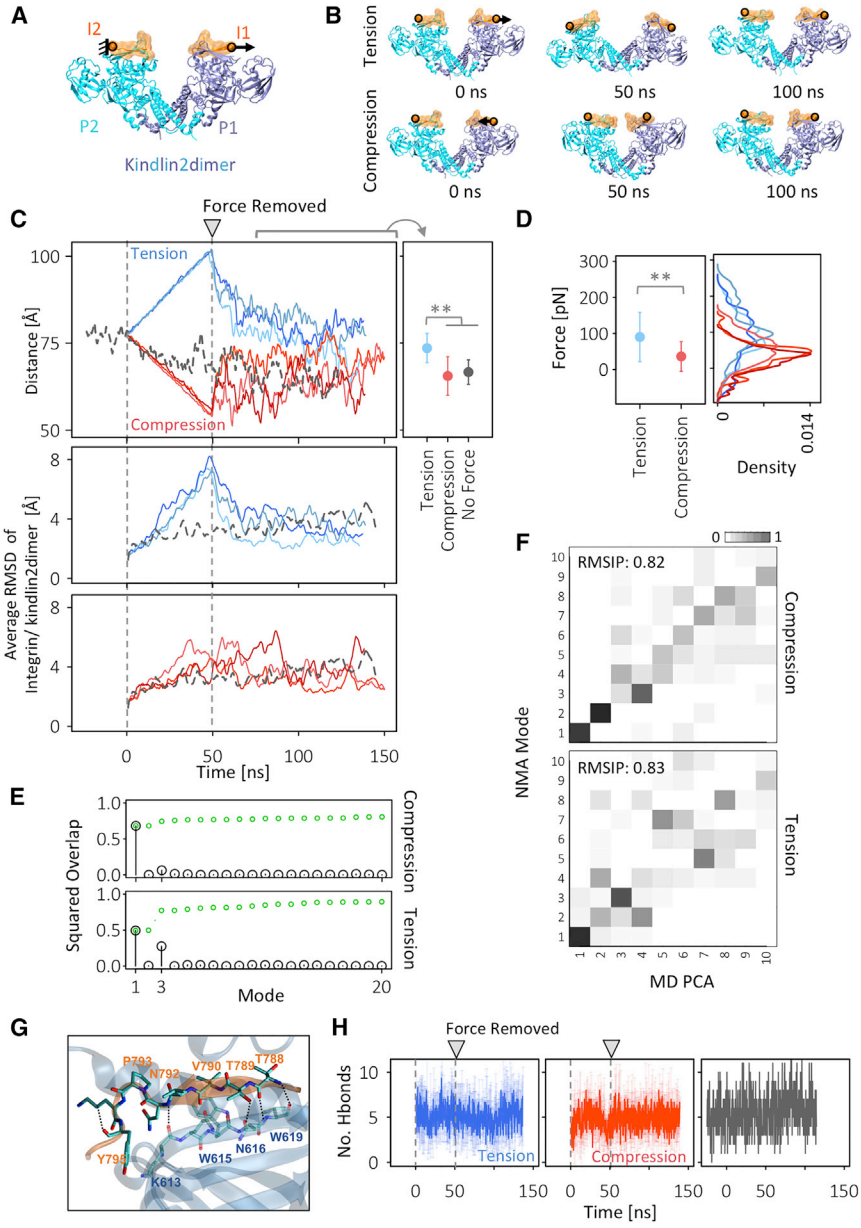

FIGURE 3 The response of the kindlin2dimer to forces on integrins. (*A*) A schematic representation of the forces applied on the integrin-kindlin2 dimer complex (PDB: 5XQ0) consisting of two protomers (P1 and P2) is shown. Terminal integrin residues (outlined with *black circles*) were either fixed (I2) or pulled at a constant velocity (I1). (*B*) Snapshots of the trajectory of the integrin-kindlin dimer complex under force are shown. (*C*) The top shows the distance between the two end residues of integrins bound to the kindlin2dimer during tension or compression. Three independent tension and three independent compression runs are shown with various shades of blue and red, respectively. The dashed black line shows the distance between terminal integrin residues in the absence of force. The average distances and SDs are shown for the last 75 ns; these values are higher in tension (73.5 ± 4.2 Å) than in compression (65.5 ± 5.5 Å) or no-force (66.6 ± 3.5 Å) conditions; $^{**}p$-value < 1e−15. Bottom-average root mean-square deviation (RMSD) of the kindlin2dimer/integrinß1 complex from its original structure (tension: *blue*; compression: *red*) is shown. (*D*) Magnitude of forces applied to I1, averaged over time of constant velocity application (i.e., 0–50 ns) and all simulations runs (yielding $N \approx 23{,}000$), is shown. Average values and SDs are shown; forces for tension are higher than forces for compression; $^{**}p$-value < 1e−15. (*E*) Overlap analysis between the normal modes of the kindlin2dimer and the conformational difference vector between the structure of the kindlin2dimer at 0 and 50 ns in the compression and tension molecular dynamics (MD) simulations are shown. Squared overlap values identify which modes contribute to the conformational changes observed under compression and tension. Black lines and circles show the values of squared overlap, and green circles show the cumulative values of squared overlap. Only nontrivial modes are shown. (*F*) Overlap map between the normal modes of the kindlin2dimer (NMA modes) and principal component analysis of MD simulations (MD PCA) of the kindlin2dimer under tension or compression are shown. The root mean-square inner product (RMSIP) of the two subsets (NMA and PCA MD) yields a value of 0.82 for compression and a value of 0.83 for tension. (Note that a value of 1 would indicate identical directionality.) Representative analyses are shown for one MD simulations of compression and tension. (*G*) Interaction network between kindlin2 and integrin where H-bonds are shown with dashed lines (H-bond distance and angle cutoffs are 4 Å and 30°, respectively). (*H*) Number of H-bonds between integrins I1 and I2 and kindlin2dimer under tension (5.1 ± 1.1), compression (4.8 ± 1.1), and no-force (5.5 ± 2.1) conditions. To see this figure in color, go online.

The integrin-kindlin2dimer interactions is maintained under force

Kindlin- and talin-bound integrins are constantly exposed to cytoskeletal forces because of their interaction with actin filaments (20,23,28,32,46–50). It is therefore interesting to explore whether the kindlin2dimer/integrin-β1 is stable under force and whether interactions at the integrin-kindlin interface are preserved (Fig. 3, *G* and *H*). The crystal structure of the kindlin2dimer/integrin-β1 complex revealed the interaction interface and the H-bond network between integrin-β1 and kindlin2dimer as shown in Fig. 3 *G* (14). To determine whether the kindlin2dimer is able to maintain its interactions with integrin-β1 under force, we calculated the number of H-bonds between integrins (I1 and I2 in Fig. 3 *A*) and the kindlin2dimer over the period of force application (0–50 ns) and relaxation (50–150 ns) (Fig. 3 *H*). Our results show that the H-bond interactions between integrins I1 and I2 and the kindlin2dimer do not change significantly under force (Fig. 3 *H*). Hence, we

next explored force-dependent structural fluctuations in the kindlin2dimer and how forces on integrin are transmitted to the dimer interface.

Tensile forces are transmitted to the kindlin2dimer interface

To determine the changes in dynamics of the kindlin2dimer under force, we quantified the RMSF of the kindlin2dimer residues under tension and compression and compared their values with a no-force condition (Fig. 4 *A*). We observed no significant changes in the RMSF of most residues except regions consisting of residues 289–324 and 518–563 on the kindlin2dimer (Fig. 4 *A*). We mapped these regions onto the structure of the kindlin2dimer and found that these regions correspond to the F2 subdomain at the dimer interface (Fig. 4 *B*). Specifically, these regions correspond to four α-helices that were previously identified as important regions in kindlin2 dimerization, namely, $\alpha1_{F2}$, $\alpha2_{F2}$, $\alpha4N_{F2}$, and $\alpha4C_{F2}$ (14). These regions directly precede the F3 subdomain, which binds to integrin (Fig. 4 *B*). Next, to determine specifically which regions were changing in response to force, we calculated the angles between pairs of α-helices at the dimer interface. Specifically, we calculated the angles between $\alpha1_{F2}$, $\alpha2_{F2}$, $\alpha4N_{F2}$, and $\alpha4C_{F2}$ of neighboring protomers and as we anticipated, these angles were tension dependent. The most significant force dependency was observed for the angle between $\alpha4C_{F2}$ of the two protomers, which increased linearly from 120 to 135° under tension (Fig. 4 *C*). Other force-dependent angles were also observed between $\alpha1_{F2}$, $\alpha2_{F2}$, and $\alpha4N_{F2}$ of neighboring protomers and between $\alpha4C_{F2}$ and $\alpha2_{F2}$ of

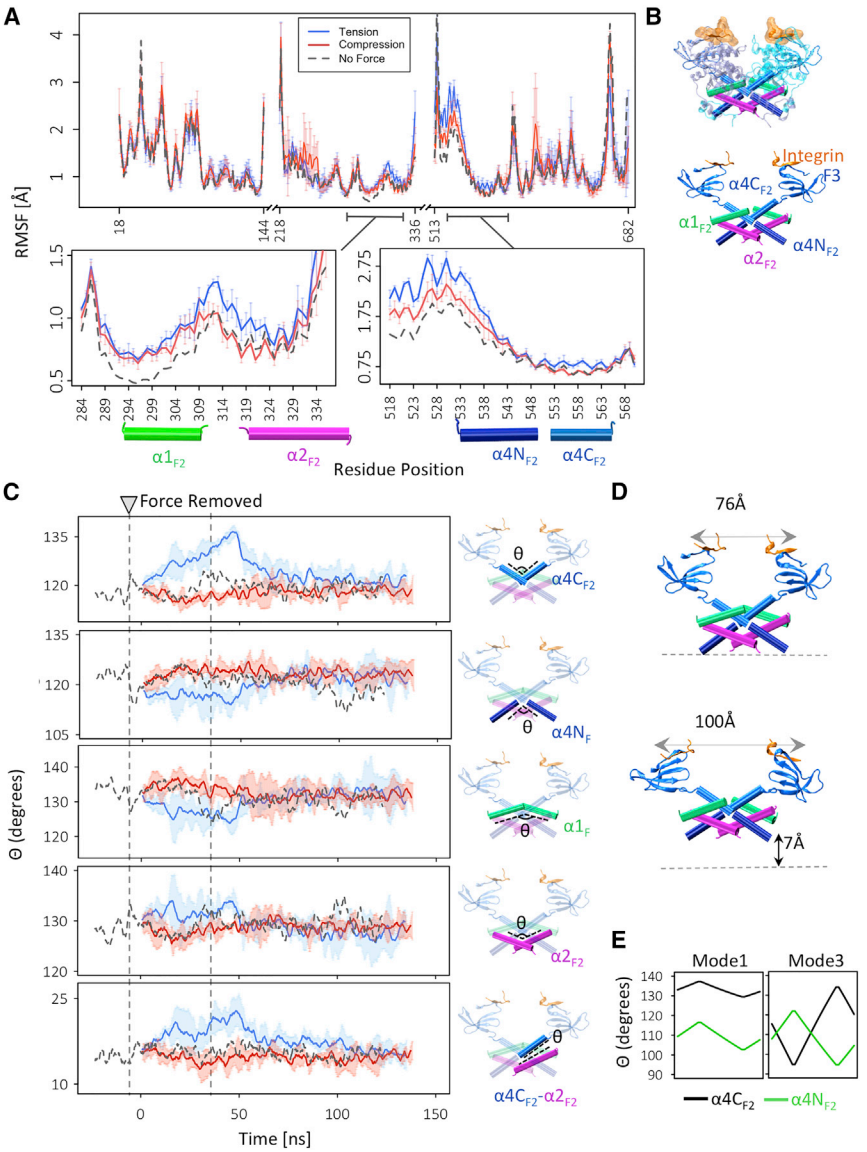

FIGURE 4 Dynamics of the kindlin2dimer under force. (*A*) Average root mean-square fluctuations (RMSF) of all residues on protomer 1 (P1) of the kindlin2dimer during force application (*top*). Regions where the RMSF is different between tension, compression, and control simulations are enlarged (*bottom*). These regions consist of α-helices that belong to the F2 subdomain of the kindlin2dimer; namely, $\alpha1_{F2}$ (residues 287–305), $\alpha2_{F2}$ (residues 310–333), $\alpha4N_{F2}$ (residues 530–545), and $\alpha4C_{F2}$ (residues 552–564). (*B*) $\alpha1_{F2}$, $\alpha2_{F2}$, $\alpha4N_{F2}$, and $\alpha4C_{F2}$ mapped onto the structure of the kindlin2dimer (*top*) are shown; the network of α-helices on the F2 subdomain and their linkage to the integrin-bound F3 subdomain through $\alpha4C_{F2}$ (*bottom*) are shown; the F3 subdomain is not entirely shown. (*C*) Angles between helices at the dimer interface over simulations time are shown; the specific angle plotted is shown to the right of each graph. The kindlin2dimer is not shown in full for visualization purposes. The relative location of each α-helix on the kindlin2dimer is shown in (*B*). (*D*) Change in end-to-end distance of integrin and the angles between $\alpha1_{F2}$, $\alpha2_{F2}$, $\alpha4N_{F2}$, and $\alpha4C_{F2}$ of neighboring monomers result in the movement of the F2 subdomain by ~7 Å in the shown direction. (*E*) Angles between $\alpha4C_{F2}$ of neighboring protomers (*black*) or $\alpha4N_{F2}$ of neighboring protomers (*green*) in the first and third nontrivial normal modes for one cycle of vibration are shown. To see this figure in color, go online.

the same protomer (Fig. 4 *C*). These changes in angles at the dimer interface also result in a ~7-Å upward shift in the position of the kindlin2dimer upon 24-Å change in the end-to-end distance of integrins under tension (Fig. 4 *D*). We also calculated the angle changes in the α4 helices for the first and third nontrivial modes, which had shown overlap with conformational changes observed in our MD simulations as indicated in Fig. 3 *E*. Indeed, in mode 1, the angle between $\alpha 4C_{F2}$ of the two protomers can oscillate between 103 and 116° during one cycle of vibration (Fig. 4 *E*; Videos S1 and S2). Similarly, the angle between $\alpha 4N_{F2}$ of the two protomers oscillates between 130 and 137° during one cycle of vibration in correlation with $\alpha 4C_{F2}$ helices (Fig. 4 *E*; Video S1). Additionally, in mode 3, the angles between $\alpha 4C_{F2}$ helices of neighboring protomers oscillate between 96 and 122° and are anticorrelated with the changes in the angle between $\alpha 4N_{F2}$ helices of neighboring protomers, which oscillate between 95 and 135° (Fig. 4 *E*; Video S2).

Finally, to determine how forces applied on integrin transfer to the dimer interface, we performed time-resolved force distribution analysis and evaluated the punctual stresses (see Materials and Methods) for all residues of α4 because this regions showed the highest change in angle under force (Fig. 5) (44,45). Our results show that punctual stresses only changed in specific residues (S550, E553, and R557) of α4 under tension (Fig. 5, *green arrows*). Under tension, residue S550 is relaxed, and the stress is transferred to E553 (Fig. 5). These results show that tensile forces on integrin are transmitted to the kindlin2dimer interface where the α-helical arrangement is adjusted to allow for the flexibility of the molecule. These results suggest that forces on integrin are transmitted to the F2 subdomain at the dimer interface.

The interaction network is shifted at the dimer interface to allow flexibility of the kindlin2dimer under force

As seen in the previous section, an extreme separation and ~15° increase in the angle between $\alpha 4C_{F2}$ helices of neighboring protomers under tension results in a decrease in punctual stresses of residue S550 and an increase of stresses in

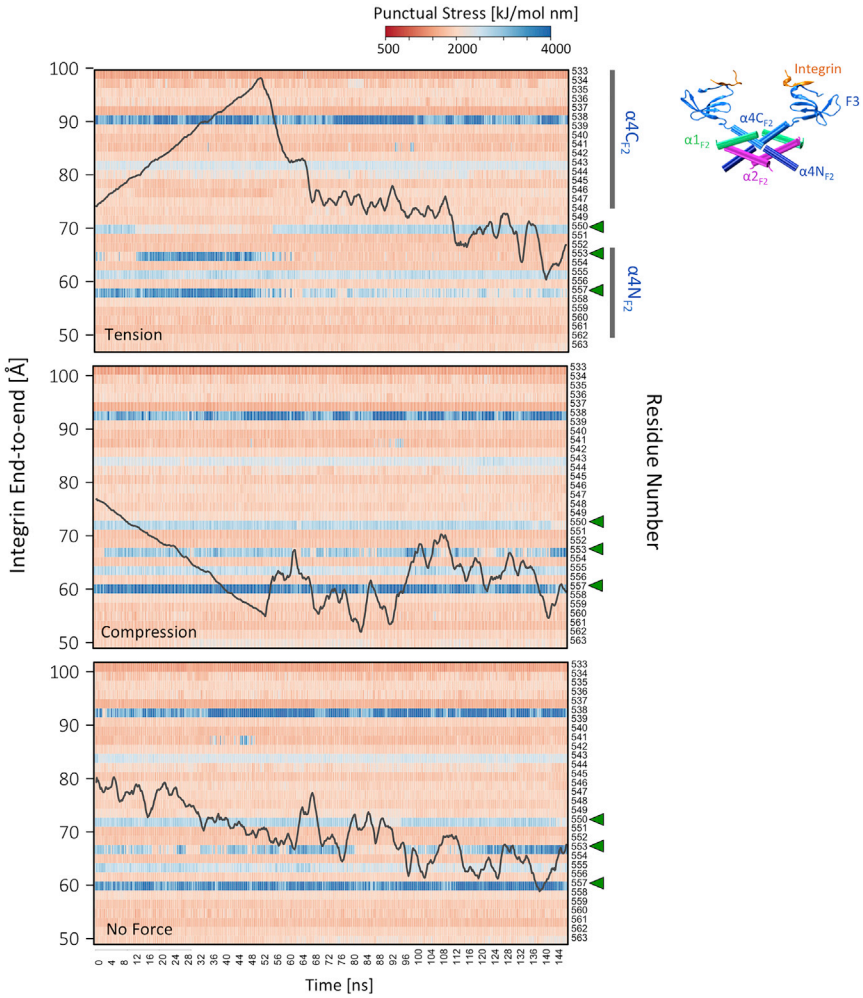

FIGURE 5 Time-resolved force distribution of dimer interface. Representative heat maps of per-residue punctual stress values over simulation time for the α_4-helix of one protomer of the kindlin2dimer are shown (P1 in Fig. 3 *A*). The distances between two integrins are also overlaid on each heat map. A representative plot is shown for each of the three conditions of tension, compression, and no force. Green arrows highlight the location of residues S550, E553, and R557, which show significant changes in punctual stresses under force. To see this figure in color, go online.

E553. To understand the consequences of such a shift in stresses, we looked more closely at these residues in our simulations. As identified in the solved crystal structure of the kindlin2dimer (PDB: 5XQ0), these residues belong to an important residue network on the F2 subdomains and were shown critical for the dimerization of kindlin2 (14). Also, these residues are conserved between different kindlin protein families (Fig. S2). This important interaction network consists of R557 on $\alpha 4N_{F2}$ of P1 or P2, which interacts with S550 on $\alpha 4C_{F2}$ of the other protomer (Fig. 6 *A*). Two such pairs exist at the dimer interface as shown in the top view of the kindlin2dimer (Fig. 6 *A*). In our models, under tensile forces, R557 switches from forming one H-bond with S550 to forming two H-bonds with E553 on $\alpha 4N_{F2}$ (Fig. 6 *B*, tension run 1–3). When tensile forces are removed while R557 is still engaged with E553, R557 does not switch back to S550 during relaxation (Fig. 6 *B*, tension run 2 and run 3). On the other hand, if the R557-E553 interaction breaks under force, R557 switches back to S550 during relaxation (Fig. 6 *B*, tension run 1). This switching is correlated with the distance between the Cα of R557 and Cα of residues S550/E553 (Fig. 6, *B* and *C*). In the crystal structure, the distance between the Cα atoms of R557 and E553 is ∼11.2 Å; at this distance, R557 interacts exclusively with S550. As tensile forces are applied, the distance between Cα atoms of R557 and E553 increases, and when this distance reaches ∼11.7 Å (first peak in Fig. 6, *B* and *C*), R557 switches from interacting with S550 to exclusively interacting with E553. When this switching occurs, the distance reaches a maximal value of 13.75 Å (second peak in Fig. 6, *B* and *C*) and is maintained even after the force is removed (unless the E553/R557 bond dissociates before force is removed) (Fig. 6 *B*, tension run 2 and run 3). Interestingly, R557 also exclusively interacts with E553 when the distances of their Cα atoms fall below ∼9.5 Å (Fig. 6 *B*, compression run 1; Fig. 6 *C*); however, this distance is not maintained when

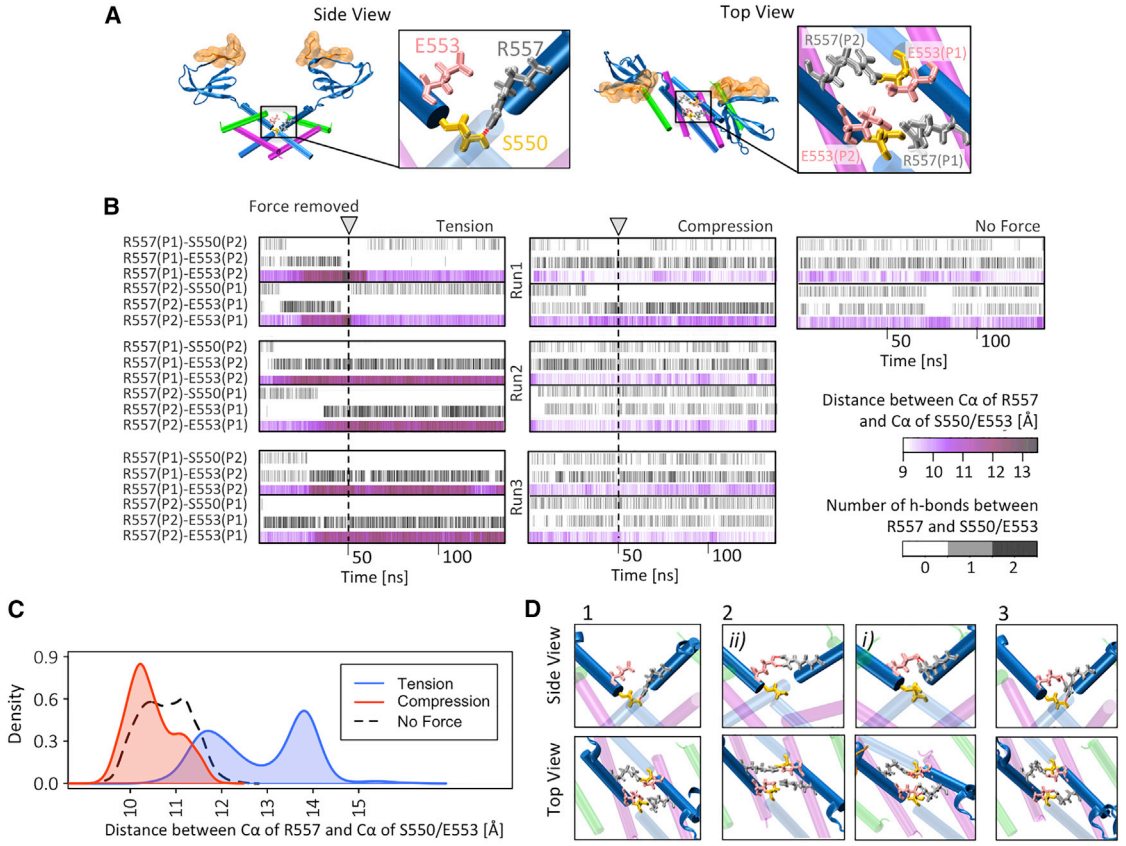

FIGURE 6 Changes in the interaction network at the kindlin2dimer interface in response to force. (*A*) The location of important interacting residue pairs R557 and S550 are shown, which are located on the F2 subdomains of separate protomers (P1 and P2) (these were identified in the crystal structure of the kindlin2dimer (PDB: 5XQ0)). A neighboring residue E553 is also shown. Two such interacting networks exist at the dimer interface (only one is shown in the side view for simplicity) (*left*). A top view of the two R557/S550/E553 interaction networks showing both pairs of residues is shown (*right*). (*B*) The number of H-bonds formed between residue R557 and residues S550/E553 over each simulation run (*gray*) and distance between R557 and residues E553 over each simulation run (*magenta*) are shown (a total of three independent runs for tension and three for compression are shown). Results for a no-force condition are also shown. (*C*) The distance between R557 and residues E553 under tension, compression, and no-force conditions is shown. (*D*) Three states of the R557/S550/E553 interaction network are shown: 1) R557 interacts exclusively with S550 (forms one H-bond), 2) R557 interacts exclusively with E553 (forms two H-bonds), and 3) R557 is shared between with S550 and E553. For each state, the side view shows only one of the two interacting networks (three residues in total), whereas the top view shows both networks (six residues in total). To see this figure in color, go online.

forces are removed. In our simulations with no force, the distance between Cα atoms of R557 and E553 fluctuates between 9 and 11.5 Å and, therefore, R557 switches between E553 (when the distance is below 9.5 Å) and S550 (when the distance is between 10.5 and 11.5 Å). At 9.5–10.5 Å, R557 is able to form one H-bond with both S550 and E553. These results suggest that the changes in the end-to-end distance of integrins directly translates to a change in the distance between the Cα of R557 and Cα of residues S550/E553, resulting in a shift in the R577-S550/E553 interaction network at the dimer interface. This interaction network can adopt four distinct states depending on the distance between the Cα of R557 and Cα of residue E553 (Fig. 6 *D*): 1) R577 interacts exclusively and forms one H-bond with S550 when Cα distance of R577 and E553 is between 10.5 and 11.5 Å; 2) R577 interacts exclusively and forms one H-bond with E553 when tensed or compressed (R577 interacts exclusively and forms two H-bonds with E553 when Cα distance of R577 and E553 is between 10.5 and 11.5 Å; R577 interacts exclusively and forms two H-bonds with E553 when Cα distance of R577 and E553 is less than 9.5 Å); and 3) R577 is shared between S550 and E553 when Cα distance of R577 and E553 is between 9.5 and 10.5 Å. The conformational shift in the two R557-S550/E553 interaction networks at the dimer interface allows for the flexibility of the kindlin2dimer/integrin-β1 complex under force.

The R557-S550/E553 conformational switch occurs under various force magnitudes

The MD simulations presented so far were all conducted at a constant velocity in which the change in the end-to-end distance between integrin tails was controlled. We next examined whether the observed behavior of the kindlin2dimer was reproducible under constant force and whether the R557-S550/E553 interaction network shift would influence the change in the end-to-end distance between integrin tails under force. To determine the response of the kindlin2dimer/integrin-β1 complex to constant force, we applied constant forces of varying magnitudes (87, 70, 35, and 17 pN) to the N-terminal end residue V787 of I1, while fixing V787 on I2. The conformational switch was indeed observed in all simulations at different time points, and the simulations were continued for at least 20 ns after the conformation switch event (Video S3). We then performed PCA as well as force distribution analysis to compare the MD trajectories of the kindlin2dimer under various force magnitudes (Fig. 7, *A* and *B*). To examine and visualize relationships between different conformations of the dimer under force, we projected the MD trajectories onto the subspace defined by the largest principal components, PC1 and PC2. For all simulations, principal components 1 and 2 (PC1 and PC2) captured more than 60% of the variance (i.e., the total mean-square displacement of atom positional fluctuations) (Fig. 7 *A*). In all simulations, the kindlin2dimer transitions between at least three distinct conformations over the simulations time. To see if forces are transmitted to α4 as they were in our simulations in which a constant velocity was applied, we performed time-resolved force distribution analysis for all constant-force simulations. We monitored the change in punctual stress values of each residue of α4 as the distance between integrins increased in response to force. In agreement with our constant-velocity simulations, an increasing distance between integrins results in a change in the punctual stresses of the R557-S550/E553 residue network, which ultimately results in a conformation switch at this interface (Fig. 7 *B*). As a result, S550 is relaxed and punctual stresses increase in E553 and R557 (Fig. 7 *C*).

Similar to our constant-velocity simulations, when pulling under a constant force, the distance between Cα of R557 and Cα of residues E553 reaches a value of ∼13.75 Å for various force magnitudes (second peak in Fig. 7 *D*). At this distance, R557 residues on each protomer interact exclusively with E553 on the neighboring protomer and form new H-bonds (Fig. 7 *E*) (two H-bonds between each R557 and E553 resulting in four new H-bonds). These new H-bonds form in all force magnitudes, including the lowest magnitude of 17 pN. To determine whether the formation of these new H-bonds alters the force response of the kindlin2dimer, we calculated the cumulative change in the distance between the two integrins before and after the distance between Cα of R557 and Cα of E553 reached a value of ∼13.75 Å on both protomers (see Materials and Methods for more details) (Fig. 7 *F*). Interestingly, the integrin distance increases much more rapidly before the conformational switch and remains constant or decreases after the switch (Fig. 7 *F*; Video S3). These results suggest that under tensile force, the kindlin2dimer may control the distance between integrin tails by shifting its R577-S550/E553 interaction network at the dimer interface. It also implies that the switching of each R557 from forming one H-bond with the neighboring S550 to forming two H-bonds with E553 may strengthen the kindlin2dimer under tensile force. The strengthening of a bond under force has previously been observed in catch bonds in other adhesion molecules (51).

DISCUSSION

Cross talk between neighboring integrins through the kindlin2dimer

The unexpected dimerization of kindlin2, as revealed in the recently solved crystal structures, proposed a mechanism by which kindlin can initiate clustering of integrins (14). The initiation of clustering could potentially be mediated either through the dimerization of kindlin2 after binding to integrins or via the simultaneous binding of two integrins to a kindlin2dimer. Either way, through NMA, we showed that the F3 subdomains of the kindlin2dimer, where the integrins bind, are dynamically cross correlated (Fig. 2). This

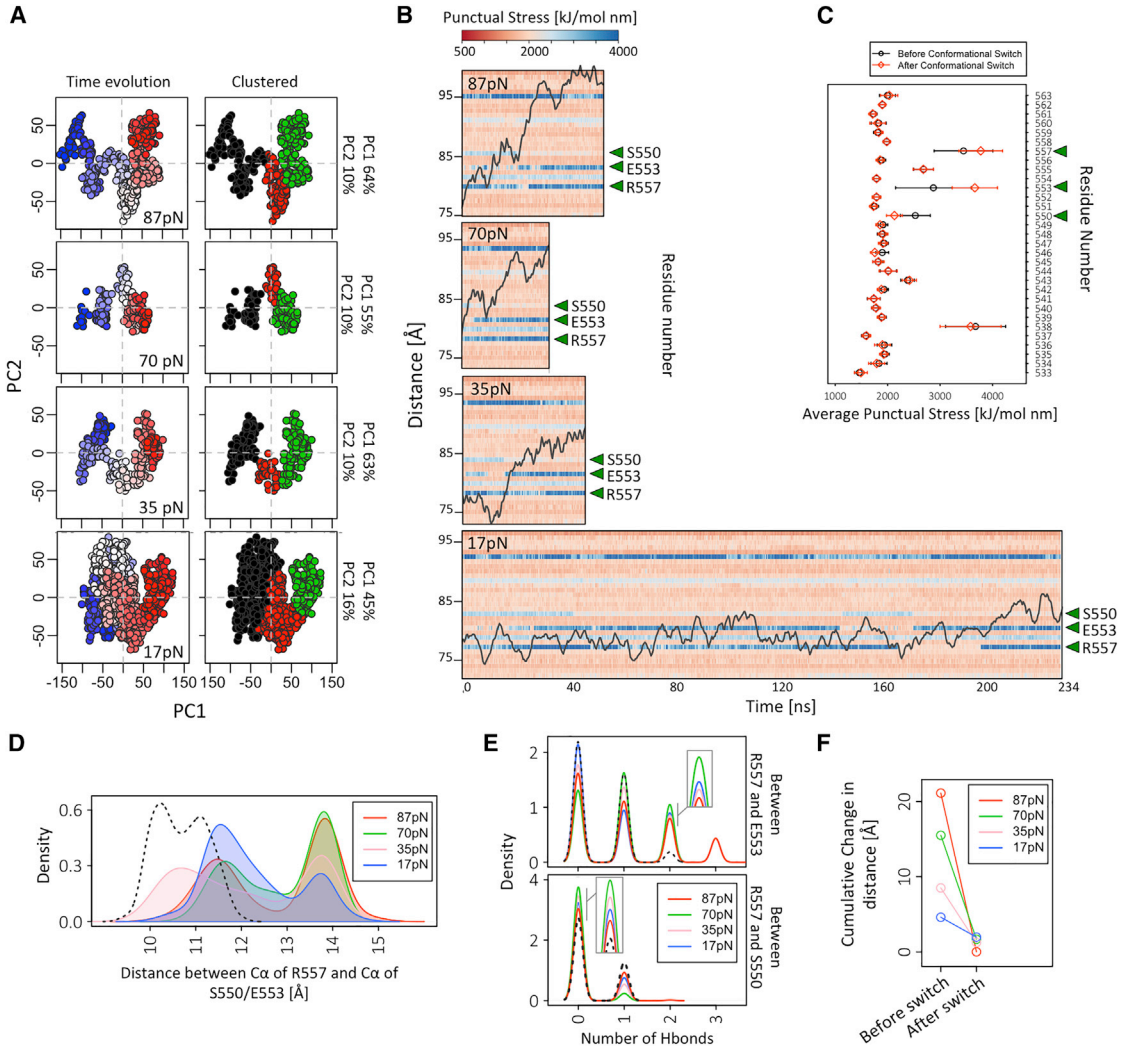

FIGURE 7 Kindlin2dimer pulled under a constant force. (*A*) Shown are a projection of molecular dynamics (MD) trajectories of the kindlin2dimer/integrin complex under forces of various magnitudes (87, 70, 35, and 17 pN) onto the subspace defined by the largest principal components 1 and 2 (PC1 and PC2). The proportion of variance (%) of PC1 and PC2 is shown to the right of each plot. Each data point represents a single frame (i.e., time point) in the MD trajectory. Data points are colored from blue (initial frame) to red (final frame) on the left. The right plots show points that are clustered in principal components space (cluster 1 (*black*) is centered around −50, cluster 2 (*red*) is centered around 0, and cluster 3 (*green*) is centered around 100). These clusters represent distinct groupings of structural conformations. (*B*) Time-resolved force distribution of dimer interface under forces of various magnitudes (87, 70, 35, and 17 pN) are shown. Representative heat maps show the per-residue punctual stress values over simulation time for the α_4-helix of one protomer (P1 in Fig. 3 *A*) in the kindlin2dimer. The distances between two integrins are also overlaid on each heat map. Green arrows highlight the location of residues S550, E553, and R557, which show a significant change in punctual stress under force. (*C*) Average per-residue punctual stresses in α_4 of both protomers (P1 and P2 in Fig. 3 *A*) before and after the conformational switch are shown (i.e., when R557 switched from interacting with S550 to E553). Green arrows highlight the location of residues S550, E553, and R557. (*D*) The distance between Cα of R557 and Cα of E553 of the neighboring protomer for both protomers (P1 and P2 in Fig. 3 *A*) under various forces is shown. The no-force condition is also shown with a dotted gray line. (*E*) The number of hydrogen bonds between R557 and E553 (*top*) or S550 (*bottom*) for both protomers (P1 and P2) under various forces is shown. The no-force condition is also shown with a dotted gray line. (*F*) Cumulative changes in the distance between integrins under force before and after the R557-S550/E553 conformational switch are shown. To see this figure in color, go online.

means that motions in one integrin can directly be translated to the other integrin through the kindlin2dimer, resulting in an intracellular cross talk between integrins. To determine which specific regions of the kindlin2dimer mediate the dynamic cross correlation observed in our NMA results, we conducted MD simulations and performed force distribution analysis along the kindlin2dimer. Our results show that forces on integrin are directly transmitted to the F2 subdomains of kindlin2 at the kindlin2dimer interface (see Figs. 4, 5, 6, and 7). These results suggest that the dynamical cross correlation between integrins is mediated by the F2 subdomains of kindlin2, which consist of four α-helices ($\alpha 1_{F2}$, $\alpha 2_{F2}$, $\alpha 4N_{F2}$, and $\alpha 4C_{F2}$; see Fig. 4) that pack together to form the dimer interface. The arrangement of these helices

is such that the lateral distance between integrins is directly correlated with the angle between these helices (Fig. 4).

Mechanosensitivity of the kindlin2dimer

In agreement with these correlations (Fig. 2), our results further show that kindlin2 can extend (elongate) and compress (shorten) in response to forces on integrin by rearranging the four α-helices at its F2 subdomains (Fig. 4). This flexibility of the kindlin2dimer is such that the lateral distance between two bound integrins can change by more than 45 Å without significant changes in the structure of the kindlin2dimer (Fig. 3 *C*) or the H-bond interactions between integrin and the kindlin2dimer (Fig. 3, *G* and *H*).

How does the dimer withstand such high strains without compromising its structure? Based on our results, we propose that a network formed by residues R577-S550/E553 at the dimer interface allows for this flexibility. Specifically, when under tension, R557 adjusts its position and switches from interacting with S550 to E553 (Figs. 5, 6, and 7). This "conformational switch" occurs for R557 on both protomers of the kindlin2dimer.When this switching occurs for the R557 residues of both protomers, the number of H-bonds between the two protomers doubles (Figs. 6 and 7 *E*), and, therefore, the dimer interface is reinforced. This reinforcement results in a resistance to further separation of the two bound integrins (Fig. 7 *F*).

The strengthening of protein interactions under tensile forces has been observed previously in several adhesion-related molecules (51). This phenomenon of force-enhanced interactions is mediated by noncovalent catch bonds whose dissociation lifetime increases with application of tensile forces (51). Although we have not determined dissociation constants in this study, we observed a similar phenomenon in the kindlin2dimer in which the number of H-bonds at the dimer interface was doubled in response to tensile force. The doubling of H-bonds was caused by a shift in the interaction network at this interface at which R557 switches from forming a single H-bond with S550 to forming two stable H-bonds with E553 (Figs. 6, 7, and 8).

Based on our results, we propose a simple model for which the motion of the kindlin2dimer is similar to a folding and self-locking shelf bracket (Fig. 8 *C*). The two brackets (i.e., $\alpha 4N_{F2}$) are highly flexible under tensile or compressive force until they are pulled apart by a fixed distance; at this point, the brackets lock into place and resist further separation. Consequently, integrins that are directly bound to the two ends of these brackets are also locked in this position. The kindlin2dimer also resembles a shelf bracket in terms of purpose. Brackets usually serve as intermediate components that fix one part to another and reinforce the two entities they connect. Similarly, we propose that the kindlin2dimer strengthens integrin clusters under cytoskeletal forces. This could be tested in vivo by mutating the conserved R577-S550/E553 residue network that is

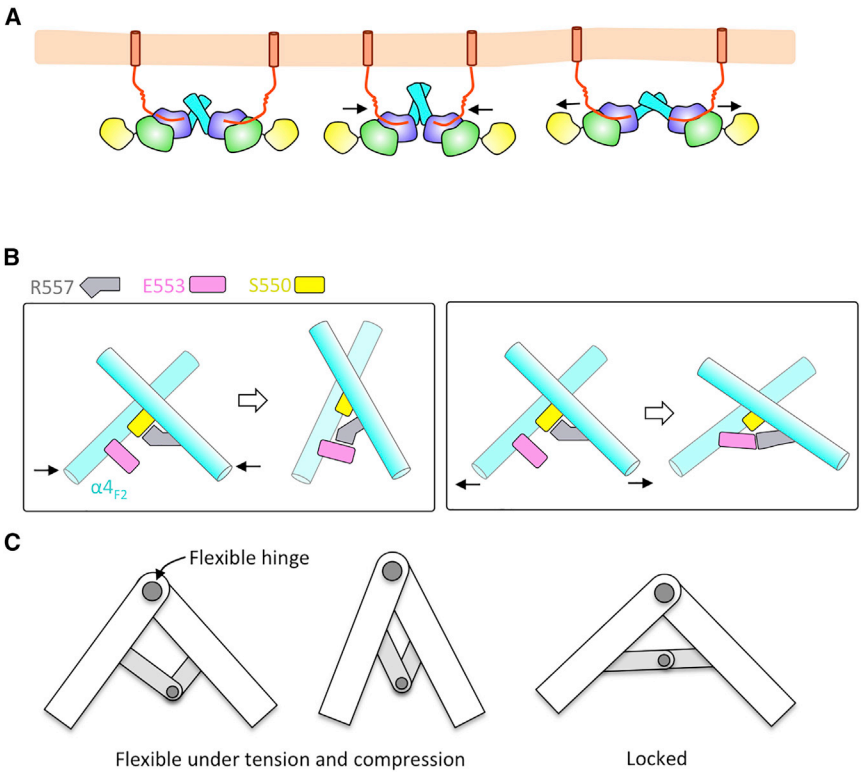

FIGURE 8 Model of cross talk among integrins through the kindlin2dimer. (*A*) Forces on integrins are directly transmitted to the kindlin dimer interface. (*B*) Consequently, a shift in the R557-E553/S550 networks at this interface allows for the flexibility of the dimer under tensile and compressive forces. Only one of the two R557-E553/S550 interacting networks is shown for simplicity. (*C*) The behavior of the kindlin2dimer under force resembles the mechanisms of a folding and self-locking shelf bracket, which is flexible in response to tension and compression, but the hinge is locked in place after the bracket reaches a desired angle. To see this figure in color, go online.

involved in the conformational switch proposed in this manuscript and testing its effect on the size of integrin clusters and forces generated within the cell.

Several studies have shown that the size of focal adhesions is proportional to adhesion strength, especially during the initial stages of myosin-mediated adhesion maturation (52–56). Based on our results, we propose that the kindlin2dimer can be involved in this by strengthening integrin clusters in response to force. Finally, we propose the kindlin2dimer as a new member of mechanosensitive adaptor proteins of the focal adhesion complex, which is involved in force bearing, force transmission, and the strengthening of integrin clusters under force.

SUPPORTING MATERIAL

Two figures and three videos are available at http://www.biophysj.org/biophysj/supplemental/S0006-3495(19)30108-0.

AUTHOR CONTRIBUTIONS

Z.J., Z.H., and M.R.K.M. designed the experiments. Z.J., Z.H., and A.R. performed the experiments. Z.J., Z.H., A.R., and M.R.K.M. analyzed the data and wrote the manuscript.

ACKNOWLEDGMENTS

We gratefully acknowledge fruitful discussions with Hengameh Shams, Mehrdad Mehrbod, and other members of the Molecular Cell Biomechanics Laboratory.

This work was supported by the National Science Foundation through grant CMMI-1538707. In addition, this research used resources of the National Energy Research Scientific Computing Center, a Department of Energy Office of Science user facility supported by the Office of Science of the United States Department of Energy under contract no. DE-AC02-05CH11231.

REFERENCES

1. Kim, M., C. V. Carman, and T. A. Springer. 2003. Bidirectional transmembrane signaling by cytoplasmic domain separation in integrins. *Science.* 301:1720–1725.
2. Xiong, J. P., T. Stehle, …, M. A. Arnaout. 2003. New insights into the structural basis of integrin activation. *Blood.* 102:1155–1159.
3. Huveneers, S., and E. H. Danen. 2009. Adhesion signaling - crosstalk between integrins, Src and Rho. *J. Cell Sci.* 122:1059–1069.
4. Hynes, R. O. 2002. Integrins: bidirectional, allosteric signaling machines. *Cell.* 110:673–687.
5. Luo, B. H., C. V. Carman, and T. A. Springer. 2007. Structural basis of integrin regulation and signaling. *Annu. Rev. Immunol.* 25:619–647.
6. Mehrbod, M., S. Trisno, and M. R. Mofrad. 2013. On the activation of integrin αIIbβ3: outside-in and inside-out pathways. *Biophys. J.* 105:1304–1315.
7. Provasi, D., A. Negri, …, M. Filizola. 2014. Talin-driven inside-out activation mechanism of platelet αIIbβ3 integrin probed by multimicrosecond, all-atom molecular dynamics simulations. *Proteins.* 82:3231–3240.
8. Shattil, S. J., C. Kim, and M. H. Ginsberg. 2010. The final steps of integrin activation: the end game. *Nat. Rev. Mol. Cell Biol.* 11:288–300.
9. Kahner, B. N., H. Kato, …, F. Ye. 2012. Kindlins, integrin activation and the regulation of talin recruitment to αIIbβ3. *PLoS One.* 7:e34056.
10. Montanez, E., S. Ussar, …, R. Fässler. 2008. Kindlin-2 controls bidirectional signaling of integrins. *Genes Dev.* 22:1325–1330.
11. Nordenfelt, P., H. L. Elliott, and T. A. Springer. 2016. Coordinated integrin activation by actin-dependent force during T-cell migration. *Nat. Commun.* 7:13119.
12. Rognoni, E., M. Widmaier, …, R. Fässler. 2016. Kindlin-2 cooperates with talin to activate integrins and induces cell spreading by directly binding paxillin. *Elife.* 5:e10130.
13. Ye, F., B. G. Petrich, …, M. H. Ginsberg. 2013. The mechanism of kindlin-mediated activation of integrin αIIbβ3. *Curr. Biol.* 23:2288–2295.
14. Li, H., Y. Deng, …, C. Yu. 2017. Structural basis of kindlin-mediated integrin recognition and activation. *Proc. Natl. Acad. Sci. USA.* 114:9349–9354.
15. Roca-Cusachs, P., A. del Rio, …, M. P. Sheetz. 2013. Integrin-dependent force transmission to the extracellular matrix by α-actinin triggers adhesion maturation. *Proc. Natl. Acad. Sci. USA.* 110:E1361–E1370.
16. Shams, H., and M. R. K. Mofrad. 2017. α-actinin induces a kink in the transmembrane domain of β3-integrin and impairs activation via Talin. *Biophys. J.* 113:948–956.
17. Sun, Z., S. S. Guo, and R. Fässler. 2016. Integrin-mediated mechanotransduction. *J. Cell Biol.* 215:445–456.
18. Yan, J., M. Yao, …, M. P. Sheetz. 2015. Talin dependent mechanosensitivity of cell focal adhesions. *Cell. Mol. Bioeng.* 8:151–159.
19. Puklin-Faucher, E., and M. P. Sheetz. 2009. The mechanical integrin cycle. *J. Cell Sci.* 122:179–186.
20. Lee, S. E., R. D. Kamm, and M. R. Mofrad. 2007. Force-induced activation of talin and its possible role in focal adhesion mechanotransduction. *J. Biomech.* 40:2096–2106.
21. Haining, A. W., M. von Essen, …, A. Del Río Hernández. 2016. All subdomains of the talin rod are mechanically vulnerable and may contribute to cellular mechanosensing. *ACS Nano.* 10:6648–6658.
22. Chen, H. S., K. S. Kolahi, and M. R. Mofrad. 2009. Phosphorylation facilitates the integrin binding of filamin under force. *Biophys. J.* 97:3095–3104.
23. Jahed, Z., H. Shams, …, M. R. Mofrad. 2014. Mechanotransduction pathways linking the extracellular matrix to the nucleus. *Int. Rev. Cell Mol. Biol.* 310:171–220.
24. Zhou, J., C. Aponte-Santamaría, …, F. Gräter. 2015. Mechanism of focal adhesion kinase mechanosensing. *PLoS Comput. Biol.* 11:e1004593.
25. Truong, T., H. Shams, and M. R. Mofrad. 2015. Mechanisms of integrin and filamin binding and their interplay with talin during early focal adhesion formation. *Integr. Biol.* 7:1285–1296.
26. Rognoni, L., J. Stigler, …, M. Rief. 2012. Dynamic force sensing of filamin revealed in single-molecule experiments. *Proc. Natl. Acad. Sci. USA.* 109:19679–19684.
27. Grashoff, C., B. D. Hoffman, …, M. A. Schwartz. 2010. Measuring mechanical tension across vinculin reveals regulation of focal adhesion dynamics. *Nature.* 466:263–266.
28. Yao, M., B. T. Goult, …, J. Yan. 2016. The mechanical response of talin. *Nat. Commun.* 7:11966.
29. Baumann, K. 2018. Mechanotransduction: Kindlin' the fate of mesenchymal stem cells. *Nat. Rev. Mol. Cell Biol.* 19:278–279.
30. Guo, L., T. Cai, …, C. Wu. 2018. Kindlin-2 regulates mesenchymal stem cell differentiation through control of YAP1/TAZ. *J. Cell Biol.* 217:1431–1451.
31. Shams, H., B. D. Hoffman, and M. R. Mofrad. 2017. The "stressful" life of cell adhesion molecules: on the mechanosensitivity of integrin adhesome. *J. Biomech. Eng.* 140:020807.
32. Seong, J., N. Wang, and Y. Wang. 2013. Mechanotransduction at focal adhesions: from physiology to cancer development. *J. Cell. Mol. Med.* 17:597–604.

33. Bledzka, K., K. Bialkowska, …, E. F. Plow. 2016. Kindlin-2 directly binds actin and regulates integrin outside-in signaling. *J. Cell Biol.* 213:97–108.

34. Karaköse, E., H. B. Schiller, and R. Fässler. 2010. The kindlins at a glance. *J. Cell Sci.* 123:2353–2356.

35. Grant, B. J., A. P. Rodrigues, …, L. S. Caves. 2006. Bio3d: an R package for the comparative analysis of protein structures. *Bioinformatics.* 22:2695–2696.

36. Schrödinger, LLC. The PyMOL Molecular Graphics System, version 2.0 (Schrödinger).

37. Jorgensen, W. L. 1983. Comparison of simple potential functions for simulating liquid water. *J. Chem. Phys.* 79:926–935.

38. Humphrey, W., A. Dalke, and K. Schulten. 1996. VMD: visual molecular dynamics. *J. Mol. Graph.* 14:33–38, 27–28.

39. Phillips, J. C., R. Braun, …, K. Schulten. 2005. Scalable molecular dynamics with NAMD. *J. Comput. Chem.* 26:1781–1802.

40. Kräutler, V., W. F. Van Gunsteren, and P. H. Hünenberger. 2001. A fast SHAKE algorithm to solve distance constraint equations for small molecules in molecular dynamics simulations. *J. Comput. Chem.* 22:501–508.

41. Skjærven, L., X. Q. Yao, …, B. J. Grant. 2014. Integrating protein structural dynamics and evolutionary analysis with Bio3D. *BMC Bioinformatics.* 15:399.

42. Bengtsson, H. 2018. matrixStats: functions that apply to rows and columns of matrices (and to vectors). R package version 0.53.1 (R Foundation for Statistical Computing).

43. Warnes, G.R. 2016. gplots: various r programming tools for plotting data. R package version 3.0.1. (R Foundation for Statistical Computing).

44. Costescu, B. I., and F. Gräter. 2013. Time-resolved force distribution analysis. *BMC Biophys.* 6:5.

45. Stacklies, W., C. Seifert, and F. Graeter. 2011. Implementation of force distribution analysis for molecular dynamics simulations. *BMC Bioinformatics.* 12:101.

46. Vogel, V., and M. Sheetz. 2006. Local force and geometry sensing regulate cell functions. *Nat. Rev. Mol. Cell Biol.* 7:265–275.

47. Lee, S. E., S. Chunsrivirot, …, M. R. Mofrad. 2008. Molecular dynamics study of talin-vinculin binding. *Biophys. J.* 95:2027–2036.

48. Golji, J., and M. R. Mofrad. 2010. A molecular dynamics investigation of vinculin activation. *Biophys. J.* 99:1073–1081.

49. Golji, J., J. Lam, and M. R. Mofrad. 2011. Vinculin activation is necessary for complete talin binding. *Biophys. J.* 100:332–340.

50. Golji, J., and M. R. K. Mofrad. 2014. The talin dimer structure orientation is mechanically regulated. *Biophys. J.* 107:1802–1809.

51. Sokurenko, E. V., V. Viola, and W. E. Thomas. 2009. Catch-bond mechanism of force-enhanced adhesion: counterintuitive, elusive, but... widespread? *Cell Host Microbe.* 4:314–323.

52. Coyer, S. R., A. Singh, …, A. J. García. 2012. Nanopatterning reveals an ECM area threshold for focal adhesion assembly and force transmission that is regulated by integrin activation and cytoskeleton tension. *J. Cell Sci.* 125:5110–5123.

53. Jamali, Y., T. Jamali, and M. R. K. Mofrad. 2013. An agent based model of integrin clustering: exploring the role of ligand clustering, integrin homo-oligomerization, integrin-ligand affinity, membrane crowdedness and ligand mobility. *J. Comput. Phys.* 244:264–278.

54. Mehrbod, M., and M. R. Mofrad. 2013. Localized lipid packing of transmembrane domains impedes integrin clustering. *PLoS Comput. Biol.* 9:e1002948.

55. Oakes, P. W., and M. L. Gardel. 2014. Stressing the limits of focal adhesion mechanosensitivity. *Curr. Opin. Cell Biol.* 30:68–73.

56. Stricker, J., Y. Aratyn-Schaus, …, M. L. Gardel. 2011. Spatiotemporal constraints on the force-dependent growth of focal adhesions. *Biophys. J.* 100:2883–2893.